Energy Constrained Transport Maximization across a Fluid Interface

Sanjeeva Balasuriya*
Department of Mathematics, Connecticut College, New London, Connecticut 06320, USA
Matthew D. Finn†
School of Mathematical Sciences, University of Adelaide, South Australia 5005, Australia
(Received 7 February 2012; published 15 June 2012)

With enhancing mixing in micro- or nanofluidic applications in mind, the problem of maximizing fluid transport across a fluid interface subject to an available energy budget is examined. The optimum cross-interface perturbing velocity is obtained explicitly in the time-periodic instance using an Euler-Lagrange constrained optimization approach. Numerical investigations which calculate transferred lobe areas and cross-interface flux are used to verify that the predicted strategy achieves optimum transport. Explicit active protocols for achieving this optimal transport are suggested.

DOI: 10.1103/PhysRevLett.108.244503 PACS numbers: 47.61.Ne, 47.10.Fg

Introduction.—Mixing fluids together efficiently at a low Reynolds number has become increasingly important over the past decade, due to enormous interest in biotechnological microfluidic devices. There is no turbulent mixing at these length scales, and diffusion occurs on a sufficiently large time scale to be ineffective by itself. To enhance reaction rates, it is often necessary to mix together two fluids—a sample and a reagent—as thoroughly as possible. Since there are a multitude of ways in quantifying mixing [1], there are similarly diverse methods to investigate optimum mixing strategies [2–5]. However, most optimum mixing theories require numerical evaluation after a point. This Letter obtains an explicit solution in a specific setting: enhancing cross-interface fluid transport subject to a given energy budget. The interface is the separating curve between the sample and reagent, which in the steady situation can be thought of as a heteroclinic manifold (a curve which simultaneously forms a stable manifold of one stagnation point, and the unstable manifold of another). Initiating advective fluid transport across such an interface is a first step towards achieving good mixing. By transporting thin and long elements of one fluid into the domain of the other, effectivity of diffusive mixing is also enhanced.

The theory for maximizing such transport is described in the "Constrained Optimization" section. Building on previous work on cross-interface flux [6–11], a constrained Euler-Lagrange approach is used to determine the time-periodic velocity which optimizes fluid transport across heteroclinic interfaces with arbitrary geometry. It is proven that the explicit solution found corresponds to transport maximization. In the "Simulations and Discussion" section, numerical simulations with a cellular flow are used to demonstrate both excellent quantitative agreement with the theory and the fact that competing strategies result in smaller flux. Several protocols (boundary membrane pulsation [12,13], cross-channel flow [14–16], and electromagnetic fields [17–20]) for achieving this optimal transport are suggested.

Constrained optimization.—We consider a 2D steady incompressible flow described by a stream function $H(\boldsymbol{x})$ in which the position $\boldsymbol{x}(t)$ of a passively advected particle satisfies

$$\dot{\boldsymbol{x}} = -\boldsymbol{J}\boldsymbol{\nabla}H(\boldsymbol{x}), \qquad \boldsymbol{J} = \begin{pmatrix} 0 & -1 \\ 1 & 0 \end{pmatrix}. \tag{1}$$

Suppose that this flow contains a heteroclinic manifold Γ connecting saddle fixed points $\boldsymbol{a}$ and $\boldsymbol{b}$ (which may be the same point). The interface Γ forms a flow barrier. If any initial condition is chosen on Γ, under (1) this trajectory approaches $\boldsymbol{a}$ and $\boldsymbol{b}$ in backwards and forwards time respectively, and therefore $t \in \mathbb{R}$ can be used to parametrize Γ through association with this trajectory $\bar{\boldsymbol{x}}(t)$. Any time shift $t \to t - \beta$ (corresponding to picking a different point on Γ as an initial condition) forms a shifted parametrization of Γ. If ℓ is the arclength measured along Γ such that $\ell = 0$ at $\boldsymbol{a}$ and $\ell = L$ (the length of Γ) at $\boldsymbol{b}$, then $d\ell/dt = |\boldsymbol{\nabla}H(\bar{\boldsymbol{x}}(t))|$. Now we seek a time-dependent perturbation to the flow of the form

$$\dot{\boldsymbol{x}} = -\boldsymbol{J}\boldsymbol{\nabla}H(\boldsymbol{x}) + \varepsilon \boldsymbol{g}(\boldsymbol{x})\cos\omega t, \tag{2}$$

which maximizes fluid transport across Γ. Here, ω is a frequency, $0 \le \varepsilon \ll 1$, and $\boldsymbol{g}$ is to be chosen so as to satisfy an energy constraint. It is well known [6,21,22] that transport occurs across Γ via lobe dynamics [23]. This transport can be explicitly characterized using Melnikov theory by defining

$$s = |\mathcal{F}\{\boldsymbol{\nabla}H(\bar{\boldsymbol{x}}(t)) \cdot \boldsymbol{g}(\bar{\boldsymbol{x}}(t))\}(\omega)|, \tag{3}$$

in which $\mathcal{F}$ represents the Fourier transform $\mathcal{F}\{h\}(\omega) := \int_{-\infty}^{\infty} h(t)e^{-i\omega t}dt$. Then, the area of each of the transported lobes is [9,24]

$$A = \varepsilon \frac{2s}{\omega} + \mathcal{O}(\varepsilon^2). \tag{4}$$

The quantity s also features in definitions of an average flux [6,7], or in an instantaneous flux [8], and thus choosing $\boldsymbol{g}$ to maximize s shall be our goal. A detailed description of the relationship between s and these various forms of flux is provided in the Supplemental Material [25].

Now, for a given $\boldsymbol{g}$, we find a time-parametrization $\bar{\boldsymbol{x}}(t)$ for Γ that ensures that the Fourier transform in (3) is real [26], and then

$$s = \left| \int_\Gamma g_\perp(\ell) \cos(\omega t(\ell)) d\ell \right|, \tag{5}$$

where $t(\ell)$ is the connection between the ℓ value at a general point $\bar{\boldsymbol{x}}(t)$ and the t-value, and $g_\perp = \boldsymbol{g} \cdot \boldsymbol{\nabla} H / |\boldsymbol{\nabla} H|$ is the velocity orthogonal to Γ.

Since only the normal component of $\boldsymbol{g}$ on the interface contributes to s we impose the kinetic energy constraint

$$\int_\Gamma g_\perp^2(\ell) d\ell = G^2 L, \tag{6}$$

where G is a given positive constant [27]. Using the Euler-Lagrange equation [28] with a Lagrange multiplier λ yields $\partial / \partial g_\perp (g_\perp \cos\omega t(\ell) - \lambda g_\perp^2) = 0$, and so $g_\perp(\ell) = \cos\omega t(\ell)/(2\lambda)$. From (6) we have $2\lambda = \pm \| \cos\omega t(\ell) \| / (G\sqrt{L})$, where the L^2 norm over Γ is defined by $\|h(\ell)\| := (\int_\Gamma h(\ell)^2 d\ell)^{1/2}$. The optimal $g_\perp$ satisfying the energy constraint is therefore [29]

$$g_\perp(\ell) = \frac{G\sqrt{L}}{\| \cos\omega t(\ell) \|} \cos\omega t(\ell). \tag{7}$$

This corresponds to a cross-interface velocity which flips back and forth across Γ in a specific way. From (5), the optimum leading-order flux is [30]

$$s_{\text{opt}} = G\sqrt{L} \| \cos\omega t(\ell) \|. \tag{8}$$

The Cauchy-Schwarz inequality applied to (5) yields $s \le \|g_\perp\| \| \cos\omega t(\ell) \| = G\sqrt{L} \| \cos\omega t(\ell) \|$, proving that (7) corresponds exactly to the flux maximum (8). Now, determining the solution as above requires knowledge of the time-parametrization which made the Fourier transform in (3) real. This is resolved as follows: (1) For some choice of $\bar{\boldsymbol{x}}(t)$, compute $g_\perp$ using (7); (2) Define $\Lambda = \mathcal{F}\{\boldsymbol{\nabla} H(\bar{\boldsymbol{x}}(t)) \cdot \boldsymbol{g}(\bar{\boldsymbol{x}}(t))\}(\omega)$; (3) If Λ is real, no reparametrization is needed; (4) If not, let $\beta = \text{Arg}\Lambda$, so that $e^{-i\beta}\Lambda = \mathcal{F}\{\boldsymbol{\nabla} H(\bar{\boldsymbol{x}}(t-\beta/\omega)) \cdot \boldsymbol{g}(\bar{\boldsymbol{x}}(t-\beta/\omega))\}(\omega)$ is real; (5) Employ the new parametrization $\bar{\boldsymbol{x}}(t-\beta/\omega)$ on Γ, replacing τ in the earlier calculations with $t - \beta/\omega$. Recalculate $t(\ell)$ based on the new parametrization; (6) Recompute $g_\perp$ in (7) using the new $t(\ell)$. This procedure unambiguously determines $g_\perp$ as a function of arclength, and is thus the energy-constrained flux-maximizing velocity.

Simulations and discussion.—We apply our method to the commonly studied Taylor-Green cellular flow [10,24,31,32] with stream function $H(x, y) = a \sin(\pi x/L) \sin(\pi y/L)$ (where L and a are positive parameters). Its flow is given by

$$\dot{x} = U(x, y) = \frac{\partial H}{\partial y}; \qquad \dot{y} = V(x, y) = -\frac{\partial H}{\partial x}, \tag{9}$$

whose flow curves are shown by the light curves in Fig. 1. The line from (0, 0) to (L, 0) is a heteroclinic trajectory Γ, with $\bar{x}(t) = (2L/\pi)\tan^{-1}(\exp[a\pi^2 t/L^2])$, $\bar{y}(t) = 0$, and $\ell = x$. So $t(x) = [L^2/(a\pi^2)] \ln(\tan[\pi x/(2L)])$, giving $\| \cos\omega t(x) \|^2 = \int_0^L \cos^2[\omega L^2/(a\pi^2) \ln(\tan[\pi x/(2L)])] dx$. For the perturbed flow

$$\dot{x} = U(x, y) + \varepsilon u(x, y, t), \qquad \dot{y} = V(x, y) + \varepsilon v(x, y, t)$$

the optimum energy-constrained choice (7) satisfies $u(x, 0, t) = 0$ and $v(x, 0, t) = g_\perp(x) \cos\omega t$, where

$$g_\perp(x) = \frac{G\sqrt{L}}{\| \cos\omega t(x) \|} \cos\left[\frac{\omega L^2}{a\pi^2} \ln\left(\tan\frac{\pi x}{2L} \right) \right]. \tag{10}$$

This function is pictured in Fig. 2 for different ω. Now $t(x)$ is odd about the midpoint $\ell = L/2$, while $g_\perp(x)$ is even. Thus, $\int_\Gamma g_\perp(\ell) \sin\omega t(\ell) d\ell = 0$ or equivalently, $\mathcal{F}\{\boldsymbol{\nabla} H(\bar{\boldsymbol{x}}(t)) \cdot \boldsymbol{g}(\bar{\boldsymbol{x}}(t))\}$ is real. No adjustment of the time-parametrization is needed.

While the theory only specifies the perturbing velocity along Γ, from a practical viewpoint an incompressible extension to the entire flow is necessary. We take $u(x, y, t) = 0$ and $v(x, y, t) = v(x, 0, t)$ (a simple extension of these normal velocities) for $0 < x < L$. Since $g_\perp(x)$ exhibits tighter and tighter oscillations as $x \to 0$ or L, using (10) is impractical in these limits. We retain $g_\perp$ only in the middle N intervals in which $\cos\omega t(x)$ is sign definite (N being an odd positive number representing the number of extrema of $g_\perp$), and use

$$v_N(x, y, t) = \begin{cases} g^\perp(x) \cos\omega t & \text{if } \gamma^- < x < \gamma^+ \\ 0 & \text{if not} \end{cases}, \tag{11}$$

where $\gamma^\pm = (2L/\pi)\tan^{-1}(\exp[\pm a\pi^3 N/(2\omega L^2)])$. Boundary membrane pulsation [12,13] can be used to achieve (11) by vibrating the top and bottom membranes in

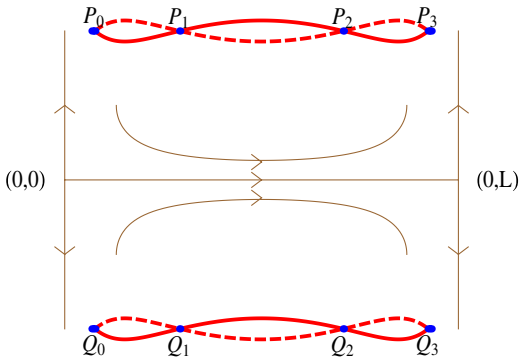

FIG. 1 (color online). Boundary membrane vibration protocol for cellular flow.

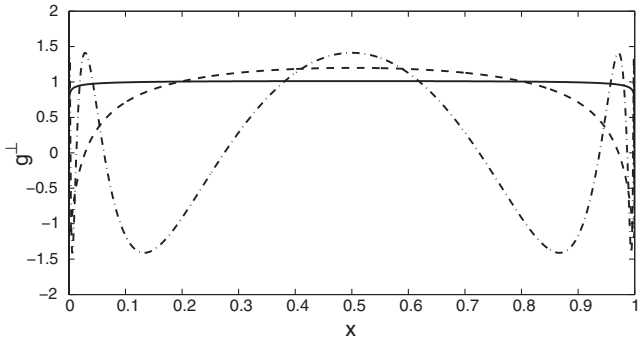

FIG. 2. Optimal $g_\perp$ for (9) with $L = 1$, $a = 1$, and $G = 1$; $\omega = 1$ (solid line), $\omega = 5$ (dashed line), and $\omega = 20$ (dot-dashed line).

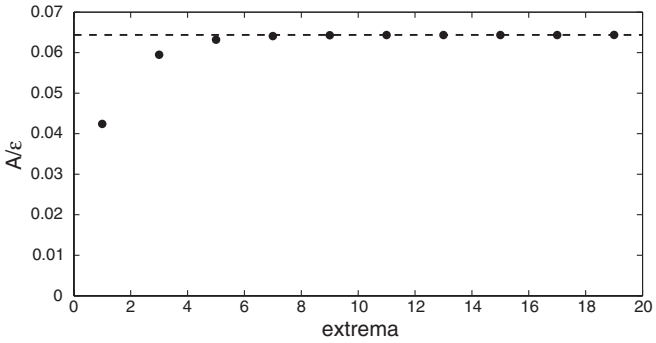

FIG. 4. The ε-normalized lobe area using the theoretically predicted velocity (11) as a function of the number of extrema N (solid dots), and the theoretical limit $N \to \infty$ (dashed line).

Fig. 1 accordingly. The membranes vibrate between the solid curve (at $t = 0$) and the dashed curve (at $t = \pi/\omega$). This picture uses the exactly computed $g_\perp(x)$ with $N = 3$, and the points P_i and Q_i are the zeroes of $g_\perp$ at which the boundary is kept fixed. Another strategy would be to have cross-channels fed via flow pumps or syringes [14–16] with the channel boundaries being the P_i and Q_i, and each channel's flow being out of phase with the adjacent channels. A third design possibility for electrorheological fluids would be to use oscillating electromagnetic fields [17–20]. For the situation pictured in Fig. 1 one could have six electrodes (one each in P_0P_1, P_1P_2, P_2P_3, Q_0Q_1, Q_1Q_2, and Q_2Q_3) governed by an alternating current, thereby approximating (11).

To numerically compute the transfer across Γ we evolve a streakline emanating from $(\gamma^-, 0)$. As the streakline is advected to the right it develops an undulation, periodically alternating between being above and below Γ for $x > \gamma^+$. Each time such a changeover happens, a lobe area A of fluid is trapped between the streakline and Γ—this is precisely what has been transported across the interface, and is readily calculated numerically.

For the following results, we set $G = L = a = 1$ and $\omega = 7\pi$. In Fig. 3 we show the variation in the transported lobe area versus the perturbation size ϵ. The linearity of the scaled transported lobe area A with respect to ϵ persists for velocities of the order of a tenth of that of the underlying cellular flow. Henceforth we take ϵ to be small enough to ensure we are firmly in the linear regime. In Fig. 4 we show how A/ϵ varies with the number of extrema N in the optimal perturbation (11). In practice taking $N = 7$ achieves 99% of the theoretical optimum.

In Fig. 5, we compare numerical and theoretical flux for different frequencies ω. The solid curve is the theoretical optimal flux (8). The circles are obtained by numerically computing A/ε of a transported lobe and then multiplying by $\omega/2$ to obtain a proxy for s using (4). The agreement is excellent.

Finally, to validate our theoretical predictions we concoct some alternative perturbation velocities that utilize the same energy budget, and demonstrate that they result in a smaller net transport across Γ. Each of these has $u = 0$, and the v candidates are

$$v = G\,\mathrm{sgn}(\cos\omega t(x))\cos\omega t, \tag{12}$$

$$v = \begin{cases} 2G\cos\omega t & \frac{3}{8}L \le x \le \frac{5}{8}L \\ 0 & \text{otherwise} \end{cases}, \tag{13}$$

$$v = \sqrt{2}G\sin\frac{\pi x}{L}\cos\omega t. \tag{14}$$

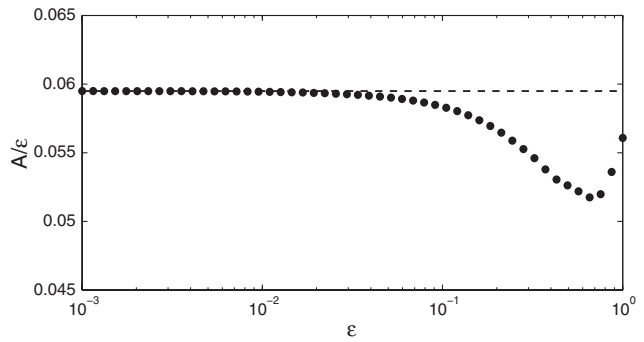

FIG. 3. The ε-normalized lobe area using (11) with $N = 7$ (solid dots), and the $\epsilon \to 0$ asymptote (dashed line).

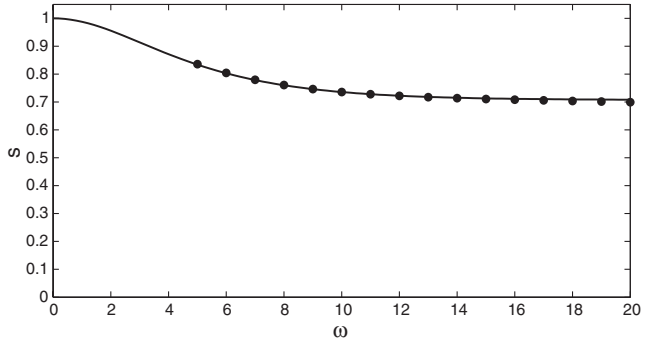

FIG. 5. The leading-order flux s (8) as a function of the frequency ω, for the optimum strategy (solid curve), in comparison with numerically evaluated lobe areas (circles).

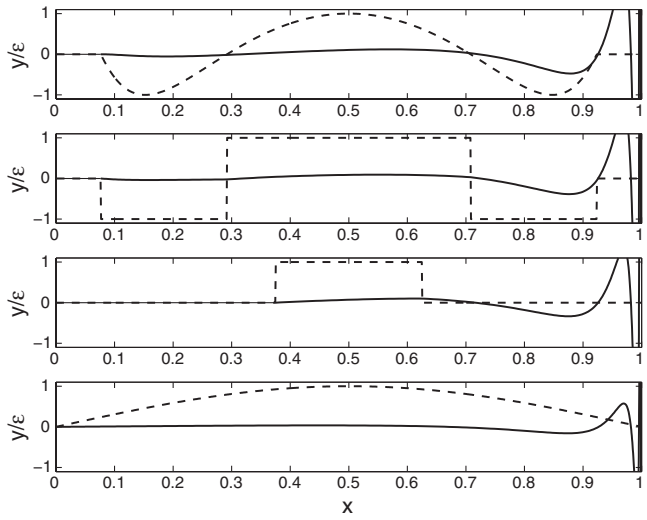

FIG. 6. Streakline snapshots (solid curves) for selected perturbation velocity profiles. Dashed lines indicate the (non-normalized) shape of the vertical perturbation velocity. From top to bottom the perturbations correspond to (11) with $N = 3$, (12) with $N = 3$, (13) and (14).

Snapshots of the corresponding streaklines are shown in the bottom three plots in Fig. 6. In order, the perturbations (12)–(14), produce a normalized area flux A/ϵ of 0.0494, 0.0397, and 0.0173, respectively. Each of these is smaller than the value $A/\epsilon = 0.0595$ corresponding to (11) with $N = 3$. These numerics offer excellent verification of the theoretically optimal strategy.

M. D. F. is grateful for support from Australian Research Council Discovery Grant No. DP0881054.

*sanjeevabalasuriya@yahoo.com
†matthew.finn@adelaide.edu.au

[1] M. D. Finn, S. M. Cox, and H. M. Byrne, J. Eng. Math. **48**, 129 (2004).
[2] G. Mathew, I. Mezić, S. Grivopoulos, U. Vaidya, and L. Petzold, J. Fluid Mech. **580**, 261 (2007).
[3] Z. Lin, J.-L. Thiffeault, and C. Doering, J. Fluid Mech. **675**, 465 (2011).
[4] L. Cortelezzi, A. Adrover, and M. Giona, J. Fluid Mech. **597**, 199 (2008).
[5] A. Vikhansky, Chem. Eng. Sci. **57**, 2719 (2002).
[6] V. Rom-Kedar, A. Leonard, and S. Wiggins, J. Fluid Mech. **214**, 347 (1990).
[7] V. Rom-Kedar and A. Poje, Phys. Fluids **11**, 2044 (1999).
[8] S. Balasuriya, Nonlinearity **19**, 2775 (2006).
[9] S. Balasuriya, Physica (Amsterdam) **202D** 155 (2005).
[10] S. Balasuriya, Phys. Fluids **17**, 118103 (2005).
[11] S. Balasuriya, Phys. Rev. Lett. **105**, 064501 (2010).
[12] J. de Jong, R. Lammertink, and M. Wessling, Lab Chip **6**, 1125 (2006).
[13] C.-H. Wang and G.-B. Lee, Biosens. Bioelectron. **21**, 419 (2005).
[14] N. Mishchuk, T. Heldal, T. Volden, J. Auerswald, and H. Knapp, Microfluid. Nanofluid. **11**, 675 (2011).
[15] P. Woias, Proc. SPIE **4560**, 39 (2001).
[16] C. Hernandez, Y. Bernard, and A. Razek, Eur. Phys. J. Appl. Phys. **51**, 20101 (2010).
[17] F. Zhang, Y. Daghighi, and D. Li, J. Colloid Interface Sci. **364**, 588 (2011).
[18] M. Z. Bazant and T. M. Squires, Phys. Rev. Lett. **92**, 066101 (2004).
[19] A. Ajdari, Phys. Rev. E **61**, R45 (2000).
[20] J. Hrdlicka, P. Cervenka, M. Pribyl, and D. Snita, Phys. Rev. E **84**, 016307 (2011).
[21] V. Rom-Kedar and S. Wiggins, Arch. Ration. Mech. Anal. **109**, 239 (1990).
[22] S. Wiggins, *Chaotic Transport in Dynamical Systems* (Springer-Verlag, New York, 1992).
[23] These lobes become narrow and elongated as time progresses [6], and in microfluidic devices with confined boundaries inevitably wrap back around to get re-entrenched. Such stretching and folding are fundamental to initiating chaotic mixing via the Smale-Birkhoff theorem, and also to promoting diffusive mixing across the elongated interfaces.
[24] S. Balasuriya, SIAM J. Appl. Dyn. Syst. **4**, 282 (2005).
[25] See Supplemental Material at http://link.aps.org/supplemental/10.1103/PhysRevLett.108.244503 for a detailed description of the relationship of the quantity s to the area flux, average flux, and instantaneous flux.
[26] When evaluating $\mathcal{F}\{\nabla H \cdot g\}$ a time shift $t \to t - \beta$ corresponds to a multiplication by $\exp(-i\beta\omega)$; there is a choice of β which rotates to the real axis.
[27] A previous attempt to maximize cross-interface flux [9] failed to account for this energy budget, and also produced an infinite rate-of-strain "solution" which was only asymptotically approached.
[28] The second term in the Euler-Lagrange equation does not appear, since the functional does not depend on $g'_\perp$, which also avoids having to use integration by parts and specify boundary conditions for $g_\perp$ at 0 and L.
[29] We have chosen the positive sign in (7); a negative sign simply flips the direction but possesses the same value for s.
[30] Elementary arguments [9] indicate that s_{opt} in (8) decays monotonically from GL at $\omega = 0^+$ to $GL/\sqrt{2}$ as $\omega \to \infty$.
[31] T. Radko, J. Fluid Mech. **668**, 76 (2010).
[32] S. Chandrasekhar, *Hydrodynamics and Hydrodynamic Stability* (Dover, New York, 1961).